Dalton Transactions

PAPER

View Article Online
View Journal | View Issue

Cite this: *Dalton Trans.*, 2025, **54**, 16241

Stability of metal–metal interactions in dinuclear Pt–Au complexes as a function of bridging Pt–arene ring electronics

Katelynn M. Farmer-Mason, Jeffrey W. Bacon and Eric S. Cueny *

A series of dinuclear Pt–Au complexes $[(bhq\text{-}Ph^{R})(PPh_3)Pt\text{–}Au(PPh_3)]^+$ (R = –H (**5**), –OMe (**5-OMe**), –F (**5-F**), and $-CF_3$ (**5-CF$_3$**)), derived from novel Pt complexes (**4**, **4-OMe**, **4-F**, and **4-CF$_3$**), were prepared and analyzed using solution-state NMR spectroscopy and X-ray crystallography. The persistence of three-center Pt–Au–C_{ipso} bonding interaction in solution and the migration of $[Au(PPh_3)]^+$ across electronically distinct arenes of **5**, **5-OMe**, **5-F**, and **5-CF$_3$** offers a unique opportunity to probe the intermediates of transmetallation as a function of bridging arene ring electronic properties. Analysis of the solid-state X-ray structures of these dinuclear complexes reveal that the degree of arene ring transfer is dictated by whether the $[Au(PPh_3)]^+$ bridges the Pt–benzoquinoline or the comparably more flexible Pt–Ph^R ring. Relative thermodynamic stability, evaluated *via* pyridine titrations, correlates with the electronic donating or withdrawing ability of the R group. A Hammett analysis of the K_{eq} derived from pyridine titrations reveal a linear relationship between the $\log(K_R/K_H)$ and σ_p values. Together, these studies demonstrate how arene ring electronic properties influence the structure and stability of transmetallation intermediates, important progress towards a deeper understanding of transmetallation between transition metal organometallic complexes.

Received 25th August 2025,
Accepted 10th October 2025

DOI: 10.1039/d5dt02048d

rsc.li/dalton

Introduction

Transmetallation is an important component of all cross-coupling reactions such as the Stille, Negishi, Kumada, and Suzuki–Miyaura reactions, which primarily differ in the identity of the stoichiometric transmetallation reagent. The mechanism of transmetallation between main-group based transmetallating reagents and palladium catalysts, especially tin,[1–6] silicon,[7–11] and boron[12–18] reagents, is fairly well-established. By contrast, less is known about the mechanism for substrate exchange between two transition metal organometallic complexes,[19] despite being a step in the Sonogashira reaction (transmetallation between Cu-acetylide and a Pd-catalyst).[20]

Early work studying transmetallation between transition metal organometallic complexes focused on late transition metals such as Pt and Au.[21,22] It is likely that metallophilic interactions play a role in these transmetallation reactions.[23] Based on the retention of stereochemistry at Pt in the exchange between *cis*-$[PtMe_2(PMe_2Ph)_2]$ and *cis*-$[PtCl_2(PMe_2Ph)_2]$ to generate 2 equivalents of *cis*-$[PtCl(Me)(PMe_2Ph)_2]$, Puddephatt proposed the now generally accepted cyclic (closed) transition state (or intermediate) for transmetallation.[21]

Since then, various reports have examined stoichiometric transmetallation between transition metal complexes,[23–26] explored transition metal catalyzed isomerization reactions,[27] and invoked transmetallation in cooperative catalytic reactions.[28,29] In stoichiometric transmetallation reactions, methyl, benzyl, and phenyl groups are capable of undergoing transmetallation with the appropriate combinations of transition metal complexes.[24] However, in some cases, methyl transfer occurs preferentially over phenyl group transfer.[26] Exclusive benzyl group transfer from Ir to Pt, over phenyl group transfer, has also been observed.[25] These results contrast Pd-catalyzed cross-coupling reactions using $Me_3Sn\text{–}R'$ (R′ = aryl or alkynyl groups) as the transmetallation reagent where selective R′ (over methyl group) transmetallation and subsequent cross-coupling occurs.[30–32] Cationic intermediates may also play a role in transmetallation between transition metal complexes given the observed anion and solvent effects in these reactions.[25,33]

More recently, the Chen and Martin groups have examined structural mimics of transmetallation intermediates (Fig. 1), each group leveraging chelation to hinder full transmetallation from one metal to the other.[34–39] Chen and coworkers have examined benzoquinoline (bhq) ligands while Martin and coworkers have used 2,6-diphenylpyridine (CNC) ligands. In both cases, a M1–M2–C_{ipso} three-center bonding interaction is present in both the solid-state and in solution. Chen's group

Department of Chemistry, Boston University, 590 Commonwealth Ave., Boston, MA 02215, USA. E-mail: ecueny@bu.edu

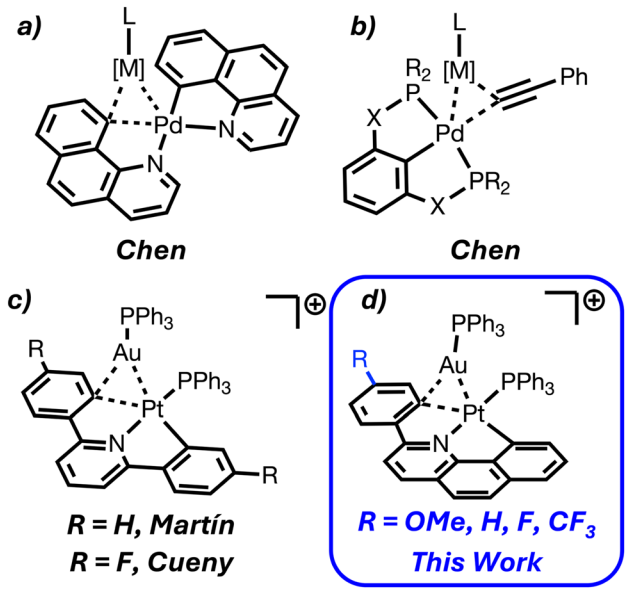

Fig. 1 (Top) Previously reported intermediates in transmetallation by Chen and coworkers. (a) [M] = Zn or Cu complexes. (b) [M] = Cu, Ag, or Au. (Bottom) Previously reported and new Pt–Au complexes as intermediates in transmetallation reported by Martin and Cueny. (c) Previous work by Martin and Cueny with 2,6-diarylpyridine ligands where R = H or F. (d) New complexes reported herein with the 2-arylbenzo[*h*]quinoline ligand where R = OMe, H, F, or CF_3.

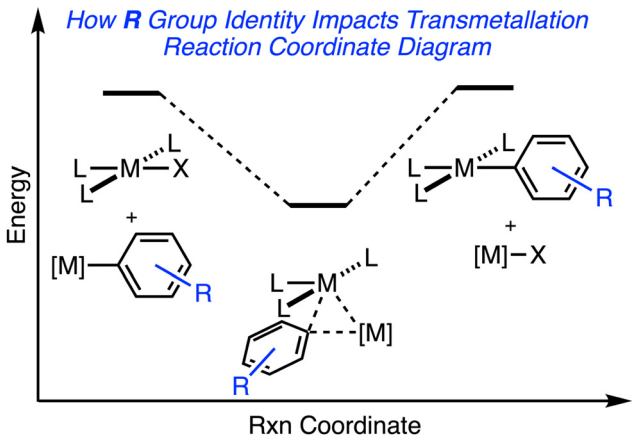

Fig. 2 Hypothetical reaction coordinate diagram for transmetallation involving a dinuclear complex with a bridging arene as an intermediate.

has also characterized the transfer of phenyl acetylide from Pd to Cu, Ag, and Au; the authors crystallographically characterized intermediates at various stages of phenyl acetylide transfer.[40]

To better understand the stability of such transmetallation intermediates, Martin and coworkers have used DFT calculations. Specifically, the authors used Energy Decomposition Analysis (EDA) to determine the stability of their dinuclear complexes.[37–39] While Chen and coworkers have employed DFT calculations, they have also used mass spectrometry in conjunction with collision-induced dissociation (CID) to measure the energy required to break up the dinuclear complexes.[33,35,36,40–42] Interestingly, by comparing the difference in CID between $[(bhq)_2Pd–Cu(IPr)]^+$ and $[(IPr)Cu(\eta^2\text{-}C_6H_6)]^+$ (IPr = 1,3-bis(2,6-diisopropylphenyl)imidazol-2-ylidene) the authors estimated the Pd(II)–Cu(I) interaction accounted for an additional ~9 kcal mol^{-1} of stability.[35]

But why expend so much effort understanding the stability of such transmetallation intermediates? In any proposed cooperative catalysis involving transmetallation, the stability of a transmetallation intermediate will have strong implications on the rate of catalysis (Fig. 2). A highly stable intermediate will decrease the steady-state concentration of active catalyst species. High energy intermediates (or transition states) may be inaccessible and hinder catalysis. This interplay of kinetic barriers and intermediate stabilities is best exemplified in alkene polymerization involving chain transfer (*i.e.* transmetallation) reagents. Chain transfer reagent metal identity (Zn *vs.* Al) and sterics of the alkyl/polymer chain undergoing exchange (1° *vs.* 2° and β-branched *vs.* non β-branched) can dictate the energetics of chain transfer from inhibition of propagation through stable intermediate formation,[43,44] successful exchange,[45–47] and high kinetic barriers leading to no observed exchange.[45,46] Thus, knowledge of the energy of transmetallation intermediates is crucial for efficient cooperative catalysis.

In previous work, we compared the binding of $[(PPh_3)Au]^+$ to $[(CNC)Pt(PPh_3)]$ (**1**) and $[(CNC^F)Pt(PPh_3)]$ (**1-F**), where CNC = 2,6-diphenylpyridine and CNC^F = 2,6-bis(4-fluorophenyl)pyridine.[48] The stability of the dinuclear complexes $[(CNC)(PPh_3)Pt–Au(PPh_3)]^+$ (**2**) and $[(CNC^F)(PPh_3)Pt–Au(PPh_3)]^+$ (**2-F**) was compared using pyridine titration experiments. Based on the K_{eq} of pyridine titrations, we found that complex **2** is more stable than **2-F**.

Herein, we seek to expand our understanding of the impact of electronic substituents on the structure and stability of transmetallation intermediates. We study electronically distinct Pt–arene groups by use of 2-arylbenzo[*h*]quinoline (bhq-Ph^R) ligands. Not only do these ligands have substantially different electronic properties amongst them, but they also bear a Pt–benzoquinoline *vs.* a Pt–Ph^R ring. Thus, there are two options for $[(PPh_3)Au]^+$ binding to the Pt-complexes, Pt–bhq *vs.* Pt–Ph^R.

We use NMR spectroscopy and X-ray crystallography to probe which of the Pt–arene ligands the $[(PPh_3)Au]^+$ binds with in both the solution- and solid-state. Using the crystal structure of the dinuclear complexes, we determine the degree of arene ring transfer using the angle between planes formed by the arene rings. We also examine the relative thermodynamic stability of these complexes by pyridine titration experiments as a function of ligand electronic properties and degree of arene transfer. Last, we use a Hammett analysis to correlate the K_{eq} from pyridine titration experiments with the σ parameters of the R groups on the Pt–Ph^R. Together, these data inform on the role of arene ring electronic properties on the structure and, more importantly, the stability of transmetallation intermediates.

Results and discussion

We begin by first synthesizing the bhq-Ph^R ligands (**3**, R = H; **3-OMe**, R = OMe; **3-F**, R = F; **3-CF$_3$**, R = CF$_3$), where **3** and **3-OMe** are known compounds.[49,50] This synthesis starts with lithiation of the appropriate bromoarene followed by selective nucleophilic addition at the 2-position of benzo[*h*]quinoline. Subsequent *in situ* oxidation leads to rearomatization of the benzo[*h*]quinoline ring yielding the desired bhq-Ph^R ligands. For **3-F**, 4-fluorophenylmagnesium bromide was reacted with benzo[*h*]quinoline *N*-oxide to produce the desired bhq-Ph^F ligand. Coordination of ligands to platinum (Scheme 1) occurs by first reacting potassium tetrachloroplatinate with the desired ligand in acetic acid at reflux over several days under N_2. The resulting Pt-dimer is then treated with excess sodium bicarbonate and triphenyl phosphine to yield the desired Pt-complexes. See the SI for synthetic details and spectroscopic characterization data.

The solid-state structures of the (bhq-Ph^R)Pt(PPh$_3$) complexes (**4**, R = H; **4-OMe**, R = OMe; **4-F**, R = F; **4-CF$_3$**, R = CF$_3$) are shown in Fig. 3. Selected bond distances and angle are shown in Table 1, for a full list of bond angles and distances see the SI. Each of the structures are quite similar, all having slightly distorted square planar geometry that is most evident in the C–Pt–C angle. The τ_4 values for each structure are quite similar (~0.17–0.18).[51] The only substantive difference in these structures is the systematic increase in the Pt–C$_{PhR}$ bond length going from R = OCH$_3$ to CF$_3$, which is interesting considering that the bond strength of Pt–C bonds is expected to be higher with electron withdrawing groups.[52–54] However, because of the extended conjugation of the 2-arylbenzo[*h*]quinoline ligand, the electron withdrawing groups can pull electron density from both the aryl and benzo[*h*]quinoline sides of the ligand, more on this subject later. None of the N–Pt–P bond angles are exactly 180° and all are quite similar. However, the PPh$_3$ group leans in different directions, towards the benzo[*h*]quinoline for R = CF$_3$ and F and towards the aryl group for R = H and OCH$_3$, which could be a result of changes in the Pt–C$_{PhR}$ bond lengths.

Synthesis and spectroscopic characterization of dinuclear Pt–Au complexes

With the Pt-complexes in hand, we set out to synthesize the Pt–Au dinuclear complexes, [(bhq-Ph^R)(PPh$_3$)Pt–Au(PPh$_3$)][OTf] (**5**, R = H; **5-OMe**, R = OMe; **5-F**, R = F; **5-CF$_3$**, R = CF$_3$). We began these investigations with the synthesis of dinuclear complex **5** from mononuclear complex **4**. Using a method similar to the syntheses of **2** and **2-F**,[38] we reacted **4** with *in situ* generated [(PPh$_3$)Au]$^+$ (Scheme 2). NMR spectroscopic evidence supports that the desired dinuclear complex was generated. ^{31}P{^{1}H} NMR spectroscopy revealed two new peaks, both of which contain Pt-satellites, indicating the cationic gold fragment binds to the Pt–arene ring. Because the two sides of the Pt-complex are asymmetric in **4**, the ^{1}H NMR spectrum of **4** contains two peaks associated with the protons alpha to Pt (Table 2), which are easily identifiable (they bear Pt-satellites) and undergo a characteristic upfield shift upon coordination of [(PPh$_3$)Au]$^+$ to the Pt–arene ligand as observed with **2** and **2-F**. In the ^{1}H NMR spectrum of **5**, both alpha protons undergo an upfield shift of 0.13 ppm and 0.19 ppm compared to **4**. Based on the upfield shift of both alpha protons, we conclude that the [(PPh$_3$)Au]$^+$ can migrate between both Pt–arene rings

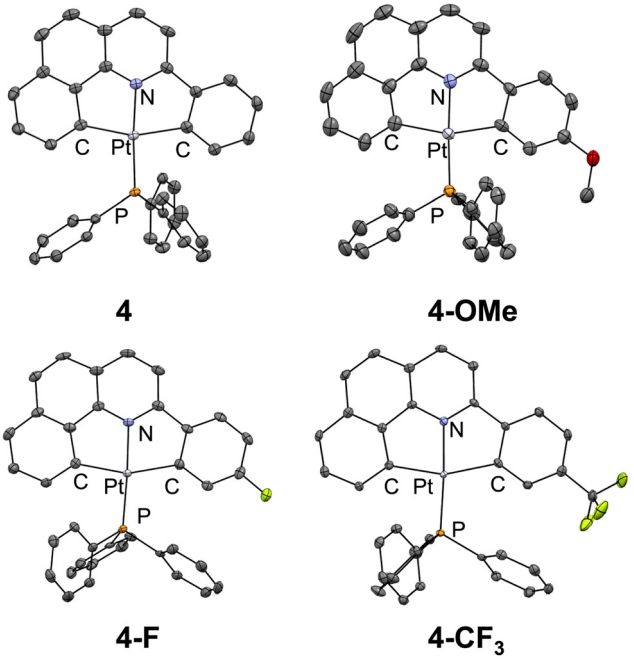

Fig. 3 Crystal structures of the monometallic (bhq-Ph^R)Pt(PPh$_3$) complexes (**4**, **4-OMe**, **4-F**, and **4-CF$_3$**). Hydrogens and solvent are omitted for clarity. Thermal ellipsoids are shown at the 50% probability level.

Table 1 Selected bond distances and angles for mononuclear Pt-complexes

	Pt–C$_{PhR}$ & Pt–C$_{bhq}$ (Å)	Pt–N (Å)	Pt–P (Å)	N–Pt–P C–Pt–C (°)
4	2.087(3) 2.097(3)	2.016(3)	2.2210(7)	174.88(8) 159.41(12)
4-OMe	2.064(7) 2.101(7)	2.032(6)	2.2176(15)	176.10(16) 159.5(3)
4-F	2.093(5) 2.084(5)	2.016(4)	2.2240(13)	176.86(13) 159.0(2)
4-CF$_3$	2.109(3) 2.096(3)	2.012(2)	2.2299(7)	175.46(6) 158.24(11)

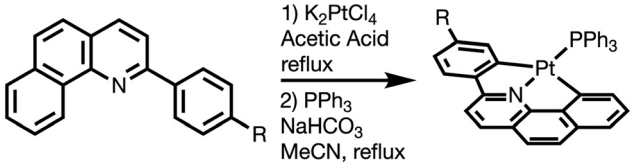

Scheme 1 Synthesis of mononuclear Pt-complexes (**4**, R = H; **4-OMe**, R = OMe; **4-F**, R = F; **4-CF$_3$**, R = CF$_3$) from bhq-Ph^R ligands (**3**, R = H; **3-OMe**, R = OMe; **3-F**, R = F; **3-CF$_3$**, R = CF$_3$).

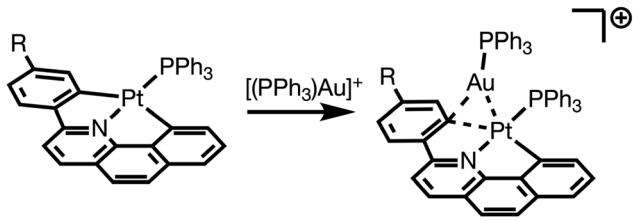

Scheme 2 Synthesis of dinuclear Pt–Au complexes (**5**, R = H; **5-OMe**, R = OMe; **5-F**, R = F; **5-CF$_3$**, R = CF$_3$) from mononuclear Pt complexes (**4**, R = H; **4-OMe**, R = OMe; **4-F**, R = F; **4-CF$_3$**, R = CF$_3$) by reaction with *in situ* generated $[(PPh_3)Au]^+$.

Table 2 Chemical shift of alpha protons of the mononuclear Pt-complexes and dinuclear Pt–Au complexes

Mononuclear & (dinuclear) complexes	Chemical shift of α-H$_{PhR}$ in ppm	Chemical shift of α-H$_{bhq}$ in ppm
1 (**2**)[38]	6.24 (6.07)	N/A
4 (**5**)	6.31 (6.18)	6.20 (6.01)
4-OMe (**5-OMe**)	6.11 (5.98)	6.21 (5.87)
4-F (**5-F**)	5.75 (6.06)[a]	6.32 (5.78)
4-CF$_3$ (**5-CF$_3$**)	6.46 (6.62)	6.43 (5.90)
1-F (**2-F**)[48]	5.80 (5.68)	N/A

[a] The peak for the proton alpha to Pt in the Pt–Ph^F ring of **4-F** can be identified by its matching coupling constant to the fluorine peak associated with the Pt–Ph^F ring in the ^{19}F NMR spectrum. For **5-F**, we identified the two alpha protons from the pyridine titration data. Upon addition of pyridine, the dinuclear complex is in equilibrium with the mononuclear Pt-complex. Based on the identity of the alpha peaks of **4-F** and the direction of the chemical shift changes upon addition of pyridine to **5-F**, we can then identify the protons alpha to Pt in the Pt–Ph^F and Pt–bhq ring of **5-F**.

of **5**. This observation is unsurprising given the electronic properties of the two Pt–arene rings of **5** are quite similar to each other and to complex **2**, and **2** undergoes an identical process in solution.

In the synthesis of **5-OMe**, similar spectroscopic data are obtained compared to **5**, and we concluded that the desired heterodinuclear complex forms and the $[(PPh_3)Au]^+$ can migrate between both Pt–arene rings of **5-OMe**. The $^{31}P\{^1H\}$ NMR spectrum of **5-OMe** reveals two new peaks, both containing Pt-satellites; the ^{1}H NMR spectrum of **5-OMe** reveals both protons alpha to Pt shift upfield upon coordination of Au. However, in the synthesis of **5-F** and **5-CF$_3$**, we observed unique spectroscopic data relative to **5** and **5-OMe**.

The $^{31}P\{^1H\}$ NMR spectra for **5-CF$_3$** was similar to **5** and **5-OMe** as two new peaks with Pt-satellites are observed indicating formation of the desired Pt–Au dinuclear complex occurs. The ^{1}H NMR spectrum of **5-CF$_3$** revealed that one proton alpha to Pt shifts upfield by 0.53 ppm and the other shifts downfield by 0.16 ppm upon coordination of $[(PPh_3)Au]^+$. The shielding effect of Au appears localized in **5-CF$_3$**; in other words, the $[(PPh_3)Au]^+$ binds exclusively to only one of the Pt–arene rings at room temperature. Based on the splitting pattern of the two alpha protons, we conclude the $[(PPh_3)Au]^+$ binds the Pt–benzo [*h*]quinoline ring over the electron deficient Pt–Ph^{CF_3} ring of **5-CF$_3$** in solution at room temperature.

To further analyze **5-CF$_3$**, we performed variable temperature NMR (VT-NMR) spectroscopy in CD_3CN over CD_2Cl_2 due to the higher boiling point of CD_3CN. The ^{1}H NMR spectra at elevated temperatures show no signs of dynamic behavior induced by increased temperature. While some peaks in the ^{1}H NMR spectrum of **5-CF$_3$** shift as the temperature increases, no broadening of any peaks are observed as would be expected if the $[(PPh_3)Au]^+$ moves between the two Pt–arene rings. It is likely that the electron withdrawing nature of the $-CF_3$ group renders the Pt–Ph^{CF_3} ring too electron poor for the $[(PPh_3)Au]^+$ to bind with it. We postulate that changes in the NMR spectra are a result of CD_3CN coordination to the complex.

For **5-F**, the $^{31}P\{^1H\}$ NMR spectroscopic data are similar to **2**, **2-F**, **5**, **5-OMe**, and **5-CF$_3$**. In the ^{1}H NMR spectrum, the protons alpha to Pt in **5-F** experience divergent chemical shift changes upon coordination of $[(PPh_3)Au]^+$. The peak associated with the alpha proton on the Pt–bhq ring shifts upfield by 0.54 ppm, while the alpha proton of the Pt–Ph^F ring shifts downfield by 0.31 ppm. At first glance, it may appear that **5-F** (with an electron deficient Pt–Ph^F ring) behaves quite similarly to complex **5-CF$_3$**. However, upon closer examination of the spectroscopic data, this conclusion is less apparent.

First, in complex **2-F**, the $[(PPh_3)Au]^+$ is able to bind to a Pt–Ph^F ring both in solution and the solid-state.[48] Thus, we do not believe that a Pt–Ph^F ring is too electron deficient to bind with $[(PPh_3)Au]^+$ in **5-F**. Second, while chemical shift changes of the alpha protons of **5-F** are divergent, the alpha proton of the Pt–Ph^F ring of **4-F** is the most upfield shifted of all the mononuclear Pt-complexes synthesized in this study (**4**, **4-OMe**, **4-F**, and **4-CF$_3$**) by ∼0.36 ppm (Table 2). Upon coordination of the $[(PPh_3)Au]^+$ the alpha proton of the Pt–Ph^F ring shifts downfield to 6.06 ppm; however, the chemical shift of this proton is within the range (Table 2) of all the alpha protons of the Pt–arene rings of the dinuclear complexes that $[(PPh_3)Au]^+$ binds with (6.18–5.78 ppm). Whereas, with **4-CF$_3$**, the chemical shift of the alpha proton on the Pt–Ph^{CF_3} ring is 6.62 ppm. For these reasons, we chose to further investigate the solution state behavior of **5-F**.

Chemical shift and splitting pattern changes are observed by ^{1}H NMR spectroscopy upon heating CD_3CN solutions of **5-F** (see SI for details). After heating, the room temperature ^{1}H NMR spectrum of **5-F** was not identical to the starting spectrum of **5-F** prior to heating. In fact, allowing CD_3CN solutions of **5-F** to stand at room temperature (or mildly elevated temperatures) reveals similar changes in the ^{1}H NMR spectra. These chemical shift changes are not observed in CD_2Cl_2 solutions of **5-F** over the same period of time suggesting the coordinating ability of CD_3CN may impact the solution-state dynamics of **5-F**. The VT NMR spectrum of **5-CF$_3$** does not show this behavior, though the amount of time **5-CF$_3$** was heated is much shorter than that of **5-F**.

Additionally, we conducted a VT-NMR study at low temperature (298 K to 188 K) of **5-F** in CD_2Cl_2 (Fig. 4) to better understand its behavior in solution. We monitored the two peaks in

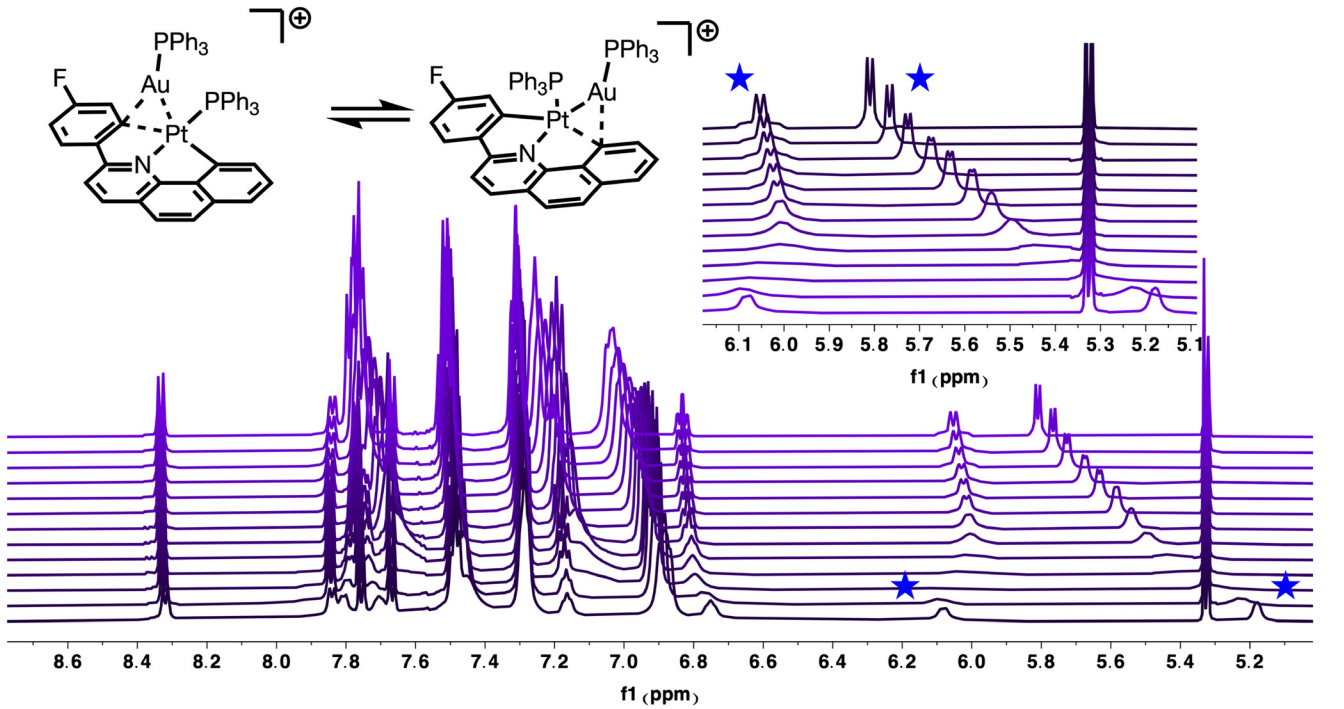

Fig. 4 Variable temperature ^{1}H NMR spectra of **5-F** in CD_2Cl_2 from 298 K (top) to 188 K (bottom). Inset shows the peaks associated with the protons alpha to Pt. Stars are also used to highlight the peaks associated with the protons alpha to Pt.

the ^{1}H NMR spectrum associated with the protons alpha to Pt. Upon cooling, substantial broadening of these peaks occurs until 213 K when both peaks broaden into the baseline, *i.e.* coalescence occurs. Using the chemical shift of alpha protons at 188 K and the coalescence temperature, we have determined the kinetic barrier to interconversion ($\Delta G^{\ddagger}$ = 10.8 kcal mol^{-1}). The kinetic barrier to interconversion is similar to that of **2** ($\Delta G^{\ddagger}$ = 8.8 kcal mol^{-1}).[38]

The low temperature NMR data demonstrate that **5-F** is fluxional at room temperature. The solid-state structural data for **5-F**, described below, support the notion that the $[(PPh_3)Au]^{+}$ can bind with both the Pt–benzo[*h*]quinoline *and* the Pt–Ph^{F} rings.

Solid-state structural characterization of dinuclear Pt–Au complexes

While the spectroscopic characterization of the solution state structure and behavior of **5**, **5-OMe**, **5-F**, and **5-CF$_3$** are informative (Fig. 5), we are also interested in the solid-state structure of these complexes for two reasons. First, we can confirm the identity of the dinuclear complexes, especially the solid-state preference of bridging arene between Pt and Au. Second, as these complexes mimic the intermediates of transmetallation, we can correlate the electronic properties of bridging arene ligands with the bonding metrics in these dinuclear complexes.

For **5-OMe**, we anticipated that the $[(PPh_3)Au]^{+}$ would bind to the comparably more flexible, and electron rich, Pt–Ph^{OMe} *vs.* the Pt–benzo[*h*]quinoline moiety in the solid-state. Indeed, the crystal structure of **5-OMe** reveals that the $[(PPh_3)Au]^{+}$

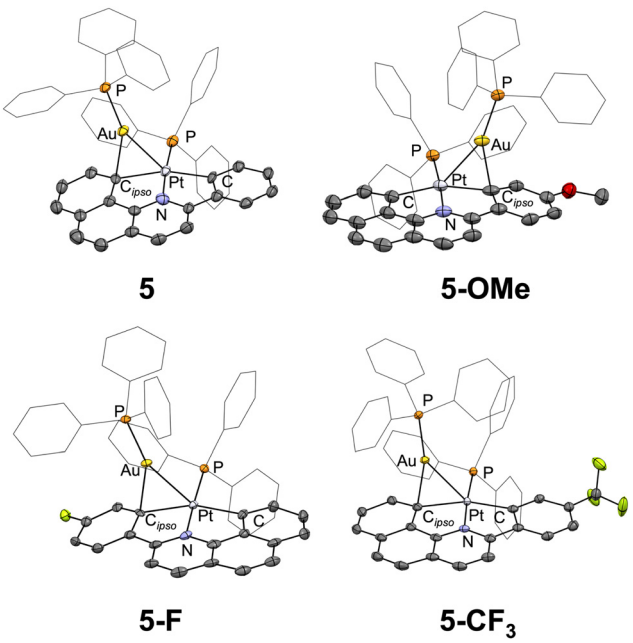

Fig. 5 Crystal structures of the dinuclear [(bhq-Ph^{R})(PPh$_3$)Pt–Au(PPh$_3$)]$^{+}$ complexes (**5**, **5-OMe**, **5-F**, and **5-CF$_3$**). Hydrogens, anions, and solvent are omitted for clarity. Thermal ellipsoids are shown at the 50% probability level. The phenyl rings of the PPh$_3$ ligands on Pt and Au are shown as wireframes for clarity. For **5** and **5-F**, only the major structure is shown (90% and 89% for **5** and **5-F**, respectively, see SI for details).

binds to the Pt–Ph^{OMe} ring. The solid-state structure of **5-OMe** contrasts that of **5-CF_3**, which reveals a preference of the $[(PPh_3)Au]^+$ to bind to the Pt–bhq moiety over the Pt–Ph^{CF_3}. Although the Pt–Ph^{CF_3} ring is more flexible than the Pt–bhq, described in more detail below, the substantial difference in electronic donating ability likely leads to this result. The structural data for **5-CF_3** is consistent with the solution-state spectroscopic observations (*vide supra*) where the $[(PPh_3)Au]^+$ binds exclusively to the Pt–bhq ring.

The solid-state structure of **5** and **5-F** are unique. The crystal structures of each complex indicates that the $[(PPh_3)Au]^+$ at least partially occupies both sides of the Pt–complex. In other words, the $[(PPh_3)Au]^+$ at least partially binds to both the Pt–bhq ring and the Pt–Ph^R ring for **5** and **5-F** (where R = H and F, respectively). For **5**, the major species (~90%) in the solid-state has the $[(PPh_3)Au]^+$ bound to the Pt–bhq ring instead of the more flexible Pt–Ph ring. The major species of **5-F** (~89%) has the $[(PPh_3)Au]^+$ bound to the Pt–Ph^F ring instead of the more electron rich Pt–bhq ring. At present, we do not know what leads to this difference in $[(PPh_3)Au]^+$ binding site. However, as we discuss below, the conjugated nature of the of the bhq-Ph^R ligands can delocalize the overall electron density across both Pt–arene rings.

While the nature of the crystal structure may be unique for these Pt–Au dinuclear complexes (**5** and **5-F**), they appear consistent with the solution-state spectroscopic data. In solution, the $[(PPh_3)Au]^+$ moves between both Pt–arenes of **5**. For **5-F**, VT-NMR spectroscopic analysis reveals that $[(PPh_3)Au]^+$ migrates between both the Pt–benzo[*h*]quinoline and Pt–Ph^F rings. Thus, the solution- and solid-state characterization data are in agreement; $[(PPh_3)Au]^+$ can bind to both the Pt–bhq and Pt–Ph^F rings of **5-F**.

Selected bond distances and angles are shown for **5**, **5-OMe**, **5-F**, and **5-CF_3** in Table 3. For all dinuclear complexes, the Pt–C bond elongates upon formation of the bridging Pt–C–Au interaction. The short Pt–Au distances are consistent with those of previously synthesized complexes **2** (2.7222(2) Å) and **2-F** (2.7430(5) Å).[38,48] Amongst the newly synthesized complexes, **5-CF_3** has the longest Pt–Au distance, which might suggest the electronic withdrawing ability of $-CF_3$ influences this structural parameter, except that **5-OMe** has the second longest Pt–Au distance (Table 3). Similarly, other structural parameters differ amongst these dinuclear complexes without much systematic variation except the C–Au–P angle which is largest for **5-CF_3** and closer to that observed in **2-F** (173.5°).[48]

Table 3 Selected bond distances and angles for dinuclear Pt–Au complexes

	Pt–Au (Å)	Pt–C (Å) of bridging Pt–arene	Au–C (Å)	C–Au–P (°)
5	2.6990(3)	2.186(5)	2.263(5)	151.30(14)
5-OMe	2.7329(4)	2.137(8)	2.242(6)	152.0(2)
5-F	2.7140(5)	2.170(7)	2.272(6)	151.12(18)
5-CF_3	2.7495(2)	2.173(3)	2.231(3)	162.92(7)

The Pt–C refers to the C_{ipso} of the arene ring bridging Pt and Au. The Au–C bond refers to the distance between Au and the C_{ipso} of the bridging arene ring. The C–Au–P refers to the angle between the C_{ipso} of the bridging arene ring, Au, and the phosphorous of the PPh_3 bound to Au.

Measurement of the degree of arene group transfer in dinuclear Pt–Au complexes

In dinuclear complexes with a bridging arene ligand, like the Pt–Au dinuclear complexes described herein, there are three important bonding modes to consider between the two metal fragments: metal–metal interactions that likely consistent of metallophilic interactions along with donor–acceptor interactions, partial arene group transfer, and full arene group transfer where the σ bond between the metal–arene interacts with the other metal (Fig. 6). We look to place the new complexes on this scale with a more quantitative measurement of the amount or degree to which the arene ring transfers from Pt to Au. We note that it is difficult to distill complicated structural distortions down to a single number. We also note that crystal packing forces (*e.g.* π stacking in the solid-state especially with the Pt–bhq rings) may impact such measurements. Despite these possible shortcomings, these measurements are valuable when comparing the extent of arene ring transfer amongst electronically distinct complexes.

Martin and coworkers reported a measurement of the degree of arene ring transfer from Pt to Au using the C_{para}–C_{ipso}–Au angle, where a 90° angle reveals no arene transfer and 180° angle reveals complete arene transfer from Pt to Au.[39] Previously, we used this method to compare the degree of arene group transfer between Pt and Au in complexes **2** and **2-F**. Due to strain in the CNC ligand upon coordination to Pt, the CNC ligand is not perfectly planar. To account for this deviation from planarity, Martin and coworkers also evaluated the C_{para}–C_{ipso}–Pt angle before and after coordination of the $[(PPh_3)Au]^+$.

We have conducted a similar analysis examining the C_{para}–C_{ipso}–Pt angle before and after coordination of the $[(PPh_3)Au]^+$ and the C_{para}–C_{ipso}–Au (Table 4). We have also examined struc-

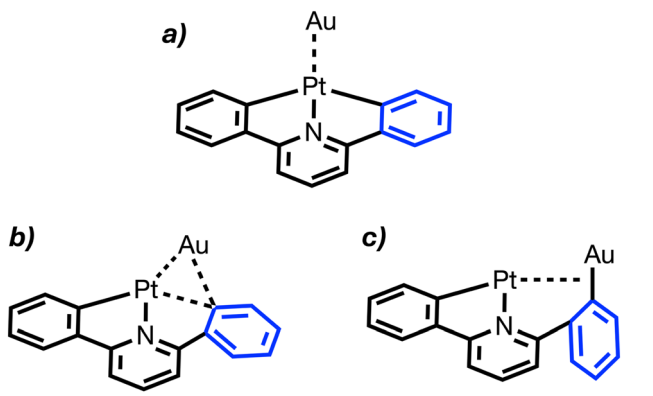

Fig. 6 Arene group transfer from Pt to Au. (a) Metal–metal interactions. (b) Partial transfer from Pt to Au. (c) Full transfer from Pt to Au.

Table 4 The C_{para}–C_{ipso}–Pt angles for the mononuclear Pt-complexes, and the C_{para}–C_{ipso}–M angles dinuclear complexes (M = Pt or Au)

	Mononuclear C_{para}–C_{ipso}–Pt	Dinuclear C_{para}–C_{ipso}–Pt	C_{para}–C_{ipso}–Au
2	168.1°	160.4°	120.1°
2-F	168.7°	159.9°	120.9°
5	167.9°	162.6°	118.5°
5-OMe	167.9°	165.5°	114.0°
5-F	167.7°	164.0°	117.4°
5-CF_3	167.9°	164.3°	112.0°

tural overlays of **2-F** and the new crystal structures reported herein (**5**, **5-OMe**, **5-F**, and **5-CF_3**) with **2** (Fig. 7). From these overlays, subtle but noticable differences in the degree of arene ring transfer can be observed with **2** apparently exhibiting the highest amount of arene ring transfer at least visually. Neither the C_{para}–C_{ipso}–Au angles nor the differences in C_{para}–C_{ipso}–Pt angle before and after $[(PPh_3)Au]^+$ binding in **2** *vs.* **2-F** suggest a significant difference in the degree of arene ring transfer.

However, even for a perfectly planar CNC-type complex, the C_{para}–C_{ipso}–Pt angle would not be 180°. The nature of the 5-member chelate formed upon metalation to Pt prohibits the C_{para}–C_{ipso}–Pt angle from reaching 180°. Thus, the C_{para}–C_{ipso}–Pt angle measures both the distortion from planarity as well as the strain of the 5-member ring. As an alternative, we measure the angle between Pt–arene rings before and after $[(PPh_3)Au]^+$ binding to determine the degree of arene ring transfer.

We use the program Mercury to calculate individual planes formed by the two Pt–arene rings (see SI for more details). We can then measure the angle between the two planes formed by the Pt–arenes also using Mercury. The monometallic Pt–complexes are not perfectly planar, so we use the angle between planes in the monometallic complex as a baseline measurement of distortion in these Pt-complexes. The difference in the measured angles between Pt–arenes in the mononuclear *vs.* the dinuclear complexes is then the degree of arene ring transfer. In contrast to the previous method for measuring the degree of arene group transfer, here 0° indicates no arene transfer from Pt to Au. As more parameters are introduced by calculating these planes, the degree of arene ring transfer assessments are prone to more error than the simpler C_{para}–C_{ipso}–M measurement. However, as we noted above, the C_{para}–C_{ipso}–M measurement captures more than just the simple bending of the Pt–arene ring out of the plane. Thus, we submit that both measurements have potential drawbacks, and we prefer the angle between planes measurement here.

Previously, we compared the degree of arene group transfer between complexes **2** and **2-F** using the C_{para}–C_{ipso}–Au angle analysis and found very little difference between them, C_{para}–C_{ipso}–Au = 120.1° and 120.9° for **2** and **2-F**, respectively.[38,48] However, using the deviation from planarity method described above, the deviation from planarity of **2** increases by 21.3° and by 7.5° in complex **2-F** upon $[(PPh_3)Au]^+$ binding. It appears that the electronic deficient, fluorinated Pt–arene rings of **2-F** lead to a significant reduction in the degree of arene group transfer.

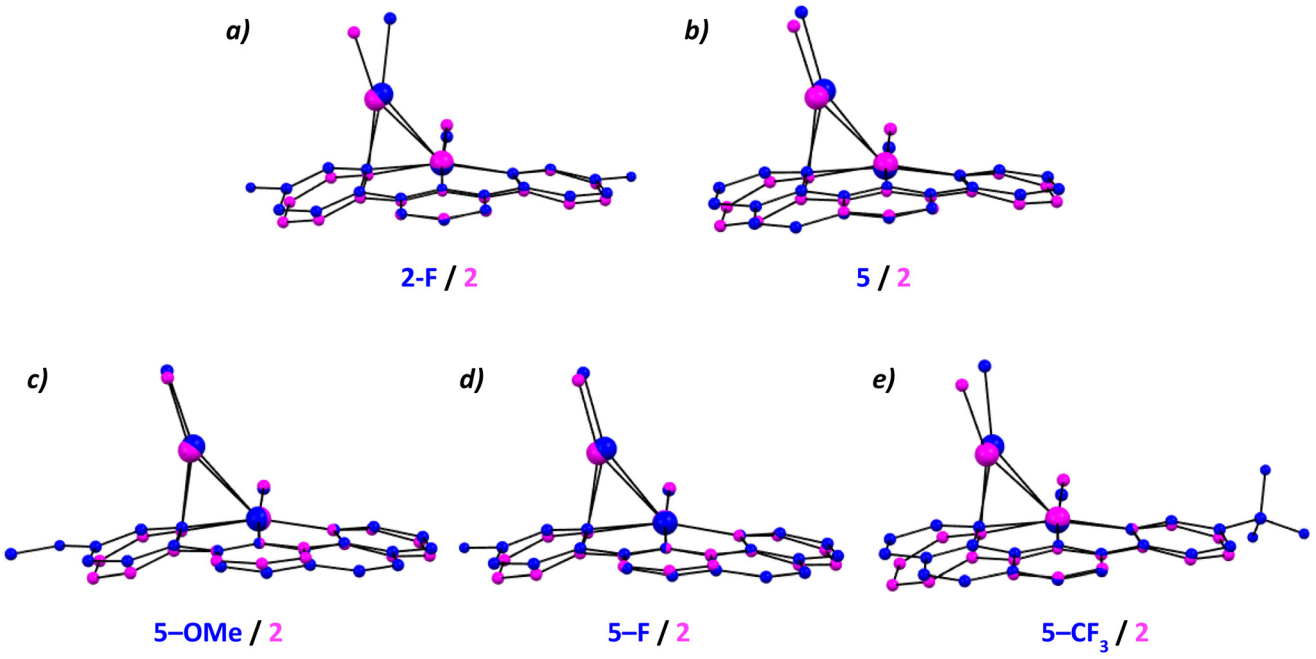

Fig. 7 Crystal structure overlays produced in Mercury. All structures are shown as a ball and stick model where solvent, anions, hydrogens, and the phenyl rings of the triphenyl phosphine ligand are omitted for clarity. All structures are compared with complex **2** shown in magenta. (a) Overlay between **2-F** (blue) and **2** (magenta). (b) Overlay between **5** (blue) and **2** (magenta). (c) Overlay between **5-OMe** (blue) and **2** (magenta). (d) Overlay between **5-F** (blue) and **2** (magenta). (e) Overlay between **5-CF_3** (blue) and **2** (magenta).

In the crystal structures of **5-CF$_3$**, the $[(PPh_3)Au]^+$ binds exclusively to the Pt–benzo[*h*]quinoline ring rather than the Pt–Ph^R ring. For **5**, $[(PPh_3)Au]^+$ binds preferentially (though not exclusively) to the Pt–benzo[*h*]quinoline ring. The resulting deviations from planarity upon $[(PPh_3)Au]^+$ binding are 4.1° and 1.6° for **5** and **5-CF$_3$**, respectively. These observations reflect how the fused rings of the Pt–bhq significantly hinder the degree of arene transfer. The crystal structure of **5-OMe** reveals the $[Au(PPh_3)]^+$ fragment binds to the Pt–Ph^{OMe} ring exclusively in the solid-state. The arene transfer of **5-OMe** (12.8°) more closely resembles that of **2** and **2-F**, 21.3° and 7.5° respectively. The lower degree of arene ring transfer in **5-OMe** *vs*. **2** likely arises from the increased rigidity of **5-OMe** enforced by the benzoquinoline ring. For **5-F**, the $[Au(PPh_3)]^+$ fragment binds preferentially to the Pt–Ph^F ring and the deviation from planarity is 12.3°, which is remarkably similar to that of **5-OMe**.

For complexes **2** *vs*. **2-F**, the substituent (H *vs*. F) on Pt–arene ring appears to dictate the degree of arene group transfer. Herein, the degree of arene ring transfer in the solid-state of **5**, **5-OMe**, **5-F**, and **5-CF$_3$** is dictated by whether the $[Au(PPh_3)]^+$ fragment binds to the Pt–bhq or the more flexible Pt–Ph^R ring. We now ask the question, what is more important in the relative thermodynamic stability of complexes **5**, **5-OMe**, **5-F**, and **5-CF$_3$**, the degree of arene group transfer or the electronic donating *vs*. withdrawing ability of the substituents on the arene ring?

Relative thermodynamic stability of dinuclear Pt–Au complexes

Martin and coworkers have studied Pt–Au, Pd–Au, Pt–Ag, and Pd–Ag di- and trinuclear complexes where the Pt or Pd was ligated by 2,6-diphenylpyridine and triphenyl phosphine. They used Energy Decomposition Analysis (EDA) to determine the stability of their di- and trinuclear complexes and made several interesting findings. The most relevant findings as they relate to the current study lie in the calculated stability of the various dinuclear complexes (Pd–Au > Pt–Au > Pd–Ag > Pt–Ag).[39] Comparing the Pd–Au and Pt–Au complexes, there is a substantial difference in the degree of arene group transfer (C_{para}–C_{ipso}–Au = 143.1° and 120.1° for Pd–Au and Pt–Au respectively). The same is true in the comparison between Pd–Ag and Pt–Ag dinuclear complexes (C_{para}–C_{ipso}–Au = 123.2° and 115.7° for Pd–Ag and Pt–Ag respectively). While many factors contribute to the stability of these dinuclear complexes, one might conclude that increasing the degree of arene group transfer increases the stability of the dinuclear complexes.

In the present study, we examine the stability of complexes bearing electron donating *vs*. withdrawing substituents and varying degrees of arene group transfer. Previously, we examined the relative thermodynamic stability of **2** *vs*. **2-F** using pyridine titrations.[48] Upon addition of various equivalents of pyridine to the dinuclear complexes, an equilibrium is established between the dinuclear Pt–Au complexes plus free pyridine and the monometallic Pt complexes plus pyridine ligated $[(PPh_3)Au]^+$ as observed *via* ^{1}H NMR spectroscopy. Using the equation $\delta_{obs} = \delta_{AX}N_{AX} + \delta_A N_A$, we obtained K_{eq} values for these pyridine titrations (K_{eq} = 1.2 and 103 for **2** and **2-F**, respectively).[55]

Herein, we conduct a nearly identical pyridine titration analysis with complexes **5**, **5-OMe**, **5-F**, and **5-CF$_3$** (see SI for details). We observe a clear trend in the relative thermodynamic stabilities of the heterodinuclear complexes (Fig. 8a). In the most electron rich complex (**5-OMe**), the $[(PPh_3)Au]^+$ exhibits the strongest binding to the Pt–arene. As electron withdrawing substituents are added, $[(PPh_3)Au]^+$ becomes progressively easier to displace from the dinuclear complexes by pyridine. Interestingly, the stability of **2** and **5** towards displacement of the $[(PPh_3)Au]^+$ by pyridine are quite similar despite their substantially different degrees of arene group transfer. For quantitative comparisons amongst these pyridine titrations, we calculated the K_{eq} (Fig. 8b) for this reaction using the known chemical shifts of the monometallic Pt-complexes, the dinuclear complexes, and the change in chemical shift as a function of equivalents of added pyridine (see SI for details).

Based on the K_{eq} values for pyridine binding, it is apparent that electronic properties rather than degree of arene group transfer dictate the stability of these dinuclear complexes. For example, **2** and **5** both have similar K_{eq} values for pyridine displacement of the $[(PPh_3)Au]^+$ (1.2 *vs*. 1.4, respectively); however, these complexes exhibit substantially different distortions from planarity (21.3° *vs*. 4.1°, respectively) upon binding $[(PPh_3)Au]^+$. For **5** and **5-CF$_3$**, these complexes exhibit similar distortions from planarity but substantial differences in pyridine displacement of the $[(PPh_3)Au]^+$. It is also worth noting that for **5-OMe** the K_{eq} of 0.33 indicates that complex **4-OMe** binds more strongly to $[(PPh_3)Au]^+$ than pyridine does.

Hammett plot analysis of pyridine titration experiments

Of note, **5-CF$_3$** features a much higher K_{eq} value (18) than **5**, **5-OMe**, and **5-F**. In solution at room temperature, the ^{1}H NMR spectroscopic data is consistent with the $[(PPh_3)Au]^+$ binding exclusively to the Pt–bhq ring for **5-CF$_3$**. Complexes **5** and **5-OMe** exhibit rapid movement of the $[(PPh_3)Au]^+$ between the Pt–benzo[*h*]quinoline and the Pt–Ph^H or Pt–Ph^{OMe} rings. Based on the solution- and solid-state structural data for complex **5-F**, movement of $[(PPh_3)Au]^+$ between the Pt–benzo[*h*]quinoline and the Pt–Ph^F ring appears possible.

Considering the structure of **5-CF$_3$**, it is surprising that the remote –CF$_3$ substituent impacts the K_{eq} so substantially. The –CF$_3$ substituent may simply withdraw electron density away from the Pt-center. Alternatively, the fact that $[(PPh_3)Au]^+$ binds to only one of the two possible Pt–arene rings may lead to a decrease in overall stability of **5-CF$_3$**. To better understand the K_{eq} values obtained for complexes **5**, **5-OMe**, **5-F**, and **5-CF$_3$**, we turned to a Hammett analysis.

Hammett analyses have long been used in the mechanistic analysis of various reactions involving organometallic complexes. Here, we use a Hammett analysis to help determine if the electron donating *vs*. withdrawing groups of complexes **5**, **5-OMe**, **5-F**, and **5-CF$_3$** (as determined by their σ parameters) correlate with their equilibrium constants in pyridine titration reactions. This analysis could inform as to whether the –CF$_3$

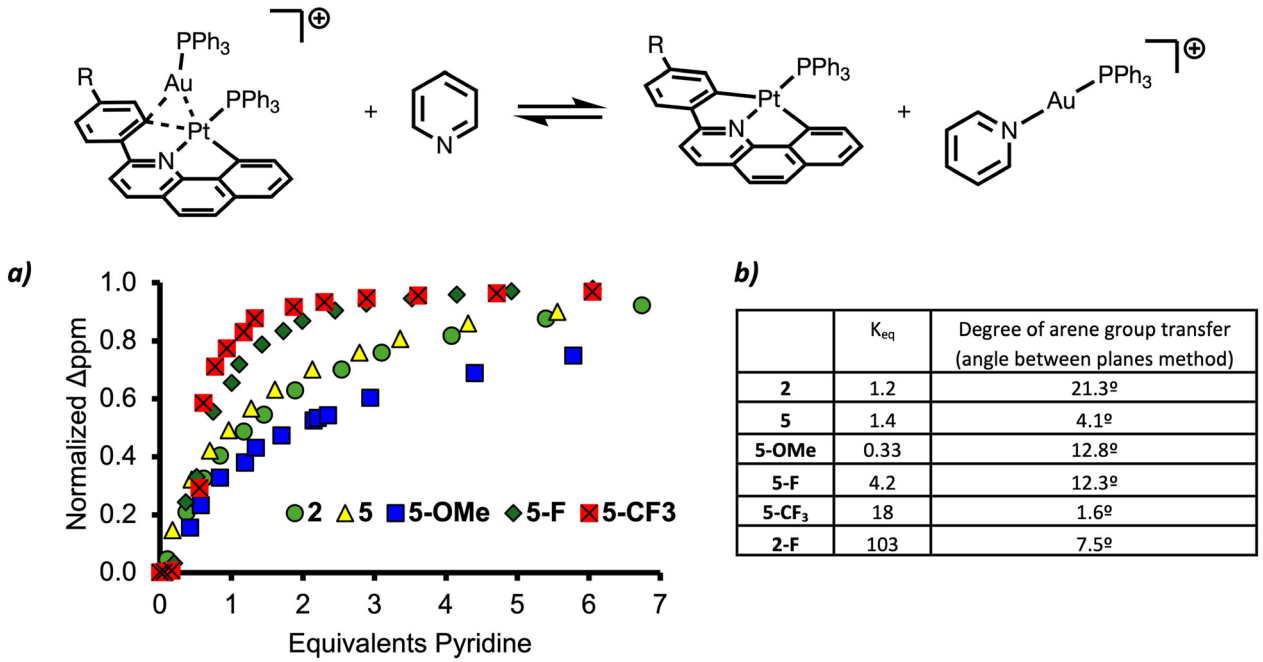

	K_{eq}	Degree of arene group transfer (angle between planes method)
2	1.2	21.3º
5	1.4	4.1º
5-OMe	0.33	12.8º
5-F	4.2	12.3º
5-CF_3	18	1.6º
2-F	103	7.5º

Fig. 8 Pyridine titration experiments involving addition of pyridine into complexes **5**, **5-OMe**, **5-F**, and **5-CF_3**. Equilibrium is established between the dinuclear Pt–Au complexes plus pyridine and the Pt mononuclear complexes **4**, **4-OMe**, **4-F**, and **4-CF_3** and pyridine ligated $[(PPh_3)Au]^+$. (a) We used the peak associated with the proton alpha to Pt in **5**, **5-OMe**, **5-F**, and **5-CF_3** and monitored the change in ppm based on the equivalents of pyridine added. We normalized the ppm change upon pyridine addition by plotting the normalized Δppm on the *y*-axis. Here, the value of zero on the *y*-axis corresponds to no change in the ppm shift (*i.e.* the chemical shift of the starting **5**, **5-OMe**, **5-F**, or **5-CF_3**). The value of one on the *y*-axis corresponds to complete dissociation of $[(PPh_3)Au]^+$ from the Pt (*i.e.* the chemical shift of **4**, **4-OMe**, **4-F**, and **4-CF_3**). (b) Table indicating the calculated K_{eq} for pyridine titrations of each complex along with the degree of arene transfer as determined by the angle between planes method described above. See SI for NMR spectra associated with the pyridine titration experiments and further information regarding K_{eq} determination and degree of arene ring transfer calculation.

group acts as simple electron withdrawing group, which would likely lead to a linear relationship between σ and $\log(K_R/K_H)$. If the fact that $[(PPh_3)Au]^+$ binds only to the Pt–bhq ring instead of both the Pt–bhq and Pt–Ph^R dictates its stability, it would likely lead to deviations in linearity in the Hammett analysis. In other words, the Hammett analysis may reveal whether something beyond the electron withdrawing ability of $-CF_3$ dictates the stability of **5-CF_3** towards pyridine titrations.

As the R groups in **5**, **5-OMe**, **5-F**, and **5-CF_3** are in the *meta* position relative to the Pt–C bond, we initially performed a Hammett analysis using the σ_m parameters. An apparent break in the plot is observed (Fig. 9a), which typically suggests a change in mechanism depending on the substituent. However, the break occurs with the $-OCH_3$ group of **5-OMe**; in the *meta* position, the $-OCH_3$ group is considered an inductively electron withdrawing group. While the $-OCH_3$ group is *meta* to the Pt–C bond, it is *para* to the rest of the benzo[*h*]quinoline ligand. As such, we also performed a Hammett analysis using the σ_p parameters and observe a linear relationship between σ_p and $\log(K_R/K_H)$ with a ρ value of 2.2 (Fig. 9b). Such discrepancies between σ_m and σ_p parameters have been described previously for derivatives of 8-aminoquinoline ligands.[56]

Previously, we used DFT calculations to show that the HOMO of **1** and **1-F** are d_{π^*} orbitals instead of d_{z^2} orbitals as is typical for d^8 square planar complexes considering the ligand sigma orbitals only.[48] Here, we performed DFT calculations on complex **4-OMe** that show the HOMO is also a d_{π^*} orbitals (Fig. 10), which is not surprising for these bhq-Ph^R has increased conjugation relative to CNC^R ligands. More importantly, these DFT calculations also reveal that the lone pairs on the oxygen of the $-OCH_3$ group contribute to the HOMO. In other words, the $-OCH_3$ group appears to act as a π donating substituent. Thus, we argue that the Hammett analysis using the σ_p parameters is more appropriate here.

The nature of the Pt–Au interactions

Given the data collected so far, in particular the pyridine titration experiments, these Pt–Au complexes are clearly quite stable in solution. In fact, **5-OMe** has a K_{eq} of 0.33 in pyridine titration experiments indicating that **4-OMe** binds to $[(PPh_3)Au]^+$ more strongly than pyridine. While metallophilic interactions provide stability to dinuclear complexes, these interactions are on the order of ~10 kcal mol^{-1}.[57,58] In other words, metallophilic interactions alone cannot explain the stability of these dinuclear complexes. Previously, Martín and coworkers conducted a detailed computational analysis of the bonding in complex **2**,[38] which is quite similar to the dinuclear complexes reported here. The EDA analysis suggests electrostatic interactions, orbital interactions, and dispersion forces all play a

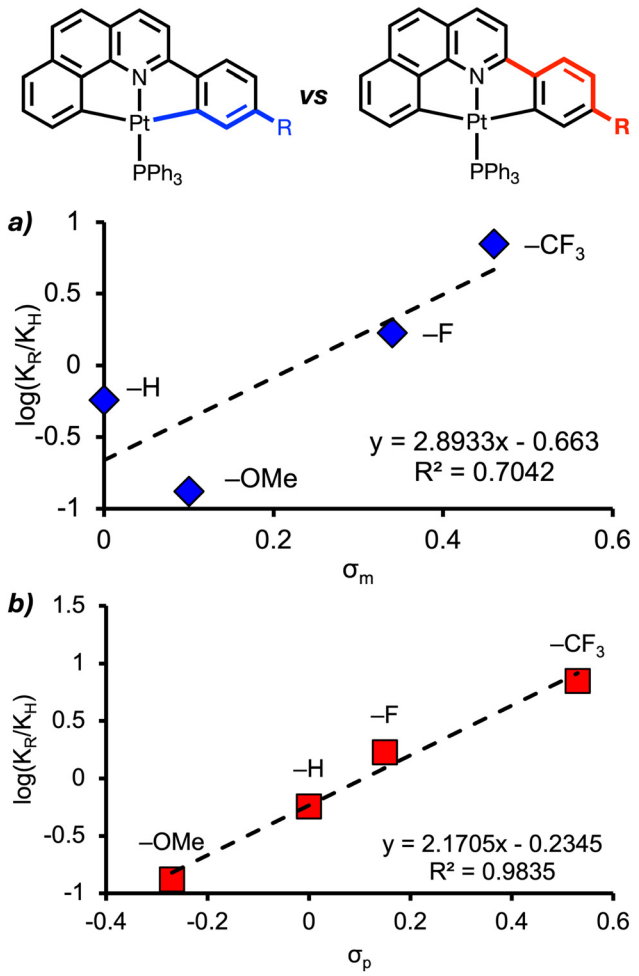

Fig. 9 Hammett analysis of complexes **4**, **4-OMe**, **4-F**, and **4-CF$_3$** (Top) Figures showing how the R groups of the Pt-complexes are *meta* to Pt and *para* to the rest of the bhq-Ph^R ligand. (a) Hammett analysis of pyridine titration experiments using the σ_m parameters. (b) Hammett analysis of pyridine titration experiments using the σ_p parameters.

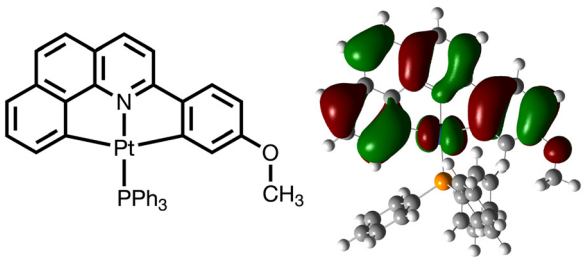

Fig. 10 DFT calculation to determine the HOMO of **4-OMe**. See SI for details on the DFT calculation.

substantial role in the stabilization of this dinuclear complex. However, even the orbital interactions are not so simple.

The largest component of the orbital stabilization involves the Pt(CNC) π orbital binding with an empty orbital centered at Au(I). We have found that the HOMO for **4-OMe** is a π orbital involving the Pt(bhq-Ph^{OMe}) fragment, which is consistent with the EDA analysis of Martín and coworkers. Interestingly, Martín and coworkers also found a not insignificant amount of backdonation from [(PPh$_3$)Au]$^+$ to (CNC)Pt(PPh$_3$). The significance of the backdonation may be enhanced by the presence of electron withdrawing groups on the Pt–arene rings, though this hypothesis requires further investigation.

To a crude approximation, one could liken the bonding between the [(PPh$_3$)Au]$^+$ fragment to (bhq-Ph^R)Pt(PPh$_3$) or (CNC^R)Pt(PPh$_3$) to that of Au binding to alkenes as alkynes. It is well established that Au complexes will bind and activate alkynes.[59,60] Of course, these dinuclear complexes have the added complexity of metallophilic interactions to consider.

Conclusions

Herein, we have described the synthesis and characterization of a series of dinuclear Pt–Au complexes (**5**, **5-OMe**, **5-F**, and **5-CF$_3$**). These dinuclear complexes are structural mimics of the intermediate in transmetallation between two transition metal complexes. We report on the solution- and solid-state structures of these dinuclear complexes as well as the relative stability of these complexes as a function of ligand electronic properties and degree of arene group transfer. To the best of our knowledge, this is the first study to systematically vary the substituents of Pt-arene rings, by adding electron donating or withdrawing groups, and study the structure and stability of Pt–Au dinuclear complexes as a function of those substituents.

In solution, the [(PPh$_3$)Au]$^+$ can migrate between the two arene rings of the bhq-Ph^R ligand except when R = CF$_3$. We conducted a VT-NMR spectroscopic analysis of **5-F**, which reveals a low kinetic barrier ($\Delta G^{\ddagger}$ = 10.8 kcal mol^{-1}) to migration of the [(PPh$_3$)Au]$^+$ between the Pt-bhq and Pt-Ph^F rings. In the solid-state, for R = OCH$_3$ the [(PPh$_3$)Au]$^+$ binds exclusively to the Pt–Ph^{OMe} ring; whereas for R = CF$_3$, the [(PPh$_3$)Au]$^+$ binds exclusively to the Pt–bhq ring. For R = H and F, both structures are present in the solid-state (*i.e.* [(PPh$_3$)Au]$^+$ binds to both the Pt–Ph^R and Pt–bhq rings).

We report a different method for determining the degree of arene group transfer from Pt to Au. Our method relies on the angles between Pt–arene rings upon Au binding instead of the C$_{para}$–C$_{ipso}$–Au angle reported previously. Using this method, we revisit previously reported complexes **2** and **2-F** along with the newly synthesized complexes **5**, **5-OMe**, **5-F**, and **5-CF$_3$**. Interestingly, the degree of arene group transfer in **5**, **5-OMe**, **5-F**, and **5-CF$_3$** does not correlate with the ligand electronic properties, only with whether or not the [(PPh$_3$)Au]$^+$ binds primarily with the Pt–Ph^R or Pt–bhq in the solid-state.

Most important to this study, we examine the relative thermodynamic stability of the newly synthesized complexes **5**, **5-OMe**, **5-F**, and **5-CF$_3$** using pyridine titration experiments. We find that the stability of these complexes does not correlate with the degree of arene group transfer as was observed by Martin and coworkers comparing Pt and Pd complexes.[39] Instead, the stability of these complexes is a function of the

electron withdrawing or donating groups of the Pt–arene. Using Hammett analysis, we find a linear correlation between the $\log(K_R/K_H)$ and σ_p.

Together, these data are crucial in understanding transmetallation between transition metal complexes as they help us understand the impact of electronic properties on the stability of transmetallation intermediates.

Author contributions

K. M. F. conducted the experiments and assisted in the writing of this manuscript. J. W. B. conducted the X-ray crystallography for this manuscript and assisted in the analysis of the crystal structures along with the writing of this manuscript. E. S. C. performed the DFT calculations and assisted in manuscript writing and editing.

Conflicts of interest

There are no conflicts to declare.

Data availability

The NMR spectroscopic data supporting the research conducted in this article are included in the supplementary information (SI). Supplementary information: geometric coordinates used in the DFT calculations supporting this research are included with this submission. See DOI: https://doi.org/10.1039/d5dt02048d.

CCDC 2453724 (**4-F**), 2453725 (**4**), 2453726 (**4-OMe**), 2453727 (**5-CF_3**), 2453728 (**5-F**), 2453729 (**4-CF_3**), 2453730 (**5-OMe**) and 2453731 (**5**) contain the supplementary crystallographic data for this paper.[61a–h]

Acknowledgements

The authors thank Boston University for funding of this project. We acknowledge the NIH S10OD028585 for the purchase of the X-ray diffractometer. We acknowledge the NSF (CHE 0443618) for the purchase of the Waters high resolution mass spectrometer. We thank Dr Paul Ralifo for help with NMR spectroscopic data collection, Dr James McNeely for help with DFT calculations, and Dr Maria del Carmen Piqueras for help with high resolution mass spectrometry.

References

1 J. Louie and J. F. Hartwig, Transmetalation, Involving Organotin Aryl, Thiolate, and Amide Compounds. An Unusual Type of Dissociative Ligand Substitution Reaction, *J. Am. Chem. Soc.*, 1995, **117**, 11598–11599.
2 A. L. Casado and P. Espinet, Mechanism of the Stille Reaction. 1. The Transmetalation Step. Coupling of R1I and R2SnBu3 Catalyzed by trans-[PdR1IL2] (R1 = C6Cl2F3; R2 = Vinyl, 4-Methoxyphenyl; L = AsPh3), *J. Am. Chem. Soc.*, 1998, **120**, 8978–8985.
3 J. A. Casares, P. Espinet and G. Salas, 14-Electron T-Shaped [PdRXL] Complexes: Evidence or Illusion? Mechanistic Consequences for the Stille Reaction and Related Processes, *Chem. – Eur. J.*, 2002, **8**, 4843–4853.
4 D. J. Cárdenas, C. Mateo and A. M. Echavarren, Synthesis of Oxa- and Azapalladacycles from Organostannanes, *Angew. Chem., Int. Ed. Engl.*, 1995, **33**, 2445–2447.
5 C. Mateo, D. J. Cárdenas, C. Fernández-Rivas and A. M. Echavarren, Isolation of Transmetalation Intermediates in the Stille Cross-Coupling Reaction of Stannanes: Synthesis of Palladacycles, Ligand Substitution, and Insertion Reactions, *Chem. – Eur. J.*, 1996, **2**, 1596–1606.
6 A. Ricci, F. Angelucci, M. Bassetti and C. Lo Sterzo, Mechanism of the Palladium-Catalyzed Metal–Carbon Bond Formation. A Dual Pathway for the Transmetalation Step, *J. Am. Chem. Soc.*, 2002, **124**, 1060–1071.
7 S. E. Denmark and R. F. Sweis, Design and Implementation of New, Silicon-Based, Cross-Coupling Reactions: Importance of Silicon–Oxygen Bonds, *Acc. Chem. Res.*, 2002, **35**, 835–846.
8 C. Mateo, C. Fernández-Rivas, A. M. Echavarren and D. J. Cárdenas, Isolation of the Transmetalation Step in the Hiyama Cross-Coupling Reaction of Organosilanes, *Organometallics*, 1997, **16**, 1997–1999.
9 E. Hagiwara, K.-i. Gouda, Y. Hatanaka and T. Hiyama, NaOH-Promoted cross-coupling reactions of organosilicon compounds with organic halides: Practical routes to biaryls, alkenylarenes and conjugated dienes, *Tetrahedron Lett.*, 1997, **38**, 439–442.
10 S. E. Denmark and J. M. Kallemeyn, Palladium-Catalyzed Silylation of Aryl Bromides Leading to Functionalized Aryldimethylsilanols, *Org. Lett.*, 2003, **5**, 3483–3486.
11 S. E. Denmark and R. F. Sweis, Fluoride-Free Cross-Coupling of Organosilanols, *J. Am. Chem. Soc.*, 2001, **123**, 6439–6440.
12 N. Miyaura, K. Yamada, H. Suginome and A. Suzuki, Novel and convenient method for the stereo- and regiospecific synthesis of conjugated alkadienes and alkenynes via the palladium-catalyzed cross-coupling reaction of 1-alkenylboranes with bromoalkenes and bromoalkynes, *J. Am. Chem. Soc.*, 1985, **107**, 972–980.
13 K. Matos and J. A. Soderquist, Alkylboranes in the Suzuki–Miyaura Coupling: Stereochemical and Mechanistic Studies, *J. Org. Chem.*, 1998, **63**, 461–470.
14 B. H. Ridgway and K. A. Woerpel, Transmetalation of Alkylboranes to Palladium in the Suzuki Coupling Reaction Proceeds with Retention of Stereochemistry, *J. Org. Chem.*, 1998, **63**, 458–460.
15 B. P. Carrow and J. F. Hartwig, Distinguishing between pathways for transmetalation in Suzuki-Miyaura reactions, *J. Am. Chem. Soc.*, 2011, **133**, 2116–2119.

16 C. P. Delaney, D. P. Marron, A. S. Shved, R. N. Zare, R. M. Waymouth and S. E. Denmark, Potassium Trimethylsilanolate-Promoted, Anhydrous Suzuki-Miyaura Cross-Coupling Reaction Proceeds via the "Boronate Mechanism": Evidence for the Alternative Fork in the Trail, *J. Am. Chem. Soc.*, 2022, **144**, 4345–4364.
17 C. P. Delaney, A. F. Zahrt, V. M. Kassel and S. E. Denmark, Effects of Ring Size and Steric Encumbrance on Boron-to-Palladium Transmetalation from Arylboronic Esters, *J. Org. Chem.*, 2024, **89**, 16170–16184.
18 A. A. Thomas and S. E. Denmark, Pre-transmetalation intermediates in the Suzuki-Miyaura reaction revealed: The missing link, *Science*, 2016, **352**, 329–332.
19 M. H. Perez-Temprano, J. A. Casares and P. Espinet, Bimetallic catalysis using transition and Group 11 metals: an emerging tool for C-C coupling and other reactions, *Chemistry*, 2012, **18**, 1864–1884.
20 R. Chinchilla and C. Nájera, The Sonogashira Reaction: A Booming Methodology in Synthetic Organic Chemistry, *Chem. Rev.*, 2007, **107**, 874–922.
21 R. J. Puddephatt and P. J. Thompson, Methyl for halogen exchange reactions between palladium(II), platinum(II), gold(I), and gold(III) complexes, *J. Chem. Soc., Dalton Trans.*, 1975, 1810–1814, DOI: 10.1039/DT9750001810.
22 R. J. Cross and J. Gemmill, Stereospecific transfer reactions of phenyl and ethynyl groups between platinum(II) atoms, *J. Chem. Soc., Dalton Trans.*, 1984, 205–209, DOI: 10.1039/DT9840000205.
23 M. H. Perez-Temprano, J. A. Casares, A. R. de Lera, R. Alvarez and P. Espinet, Strong metallophilic interactions in the palladium arylation by gold aryls, *Angew. Chem., Int. Ed.*, 2012, **51**, 4917–4920.
24 N. H. Chan, J. J. Gair, M. Roy, Y. Qiu, D.-S. Wang, L. J. Durak, L. Chen, A. S. Filatov and J. C. Lewis, Insight into the Scope and Mechanism for Transmetalation of Hydrocarbyl Ligands on Complexes Relevant to C–H Activation, *Organometallics*, 2020, **40**, 6–10.
25 L. J. Durak and J. C. Lewis, Transmetalation of Alkyl Ligands from Cp*(PMe3)IrR1R2 to (cod)PtR3X, *Organometallics*, 2013, **32**, 3153–3156.
26 S. E. Smith, J. M. Sasaki, R. G. Bergman, J. E. Mondloch and R. G. Finke, Platinum-Catalyzed Phenyl and Methyl Group Transfer from Tin to Iridium: Evidence for an Autocatalytic Reaction Pathway with an Unusual Preference for Methyl Transfer, *J. Am. Chem. Soc.*, 2008, **130**, 1839–1841.
27 A. L. Casado and P. Espinet, A Novel Reversible Aryl Exchange Involving Two Organometallics: Mechanism of the Gold(I)-Catalyzed Isomerization of trans-[PdR2L2] Complexes (R = Aryl, L = SC4H8), *Organometallics*, 1998, **17**, 3677–3683.
28 D. Wang, Y. Izawa and S. S. Stahl, Pd-catalyzed aerobic oxidative coupling of arenes: evidence for transmetalation between two Pd(II)-aryl intermediates, *J. Am. Chem. Soc.*, 2014, **136**, 9914–9917.
29 L. J. Durak and J. C. Lewis, Iridium-Promoted, Palladium-Catalyzed Direct Arylation of Unactivated Arenes, *Organometallics*, 2014, **33**, 620–623.
30 J. W. Labadie and J. K. Stille, Mechanisms of the palladium-catalyzed couplings of acid chlorides with organotin reagents, *J. Am. Chem. Soc.*, 1983, **105**, 6129–6137.
31 R. Crescenzi and C. L. Sterzo, Synthesis of metal acetylides via palladium-catalyzed carbon-metal bond formation, *Organometallics*, 1992, **11**, 4301–4305.
32 E. Viola, C. Lo Sterzo, R. Crescenzi and G. Frachey, Formation of metal σ-acetylides of Mo, W, and Ru via palladium-catalyzed metal-carbon coupling, *J. Organomet. Chem.*, 1995, **493**, 55–59.
33 D. Serra, M. E. Moret and P. Chen, Transmetalation of methyl groups supported by Pt(II)-Au(I) bonds in the gas phase, in silico, and in solution, *J. Am. Chem. Soc.*, 2011, **133**, 8914–8926.
34 E. Paenurk, R. Gershoni-Poranne and P. Chen, Trends in Metallophilic Bonding in Pd–Zn and Pd–Cu Complexes, *Organometallics*, 2017, **36**, 4854–4863.
35 R. J. Oeschger and P. Chen, Structure and Gas-Phase Thermochemistry of a Pd/Cu Complex: Studies on a Model for Transmetalation Transition States, *J. Am. Chem. Soc.*, 2017, **139**, 1069–1072.
36 R. J. Oeschger and P. Chen, A Heterobimetallic Pd–Zn Complex: Study of a d8–d10Bond in Solid State, in Solution, and in Silico, *Organometallics*, 2017, **36**, 1465–1468.
37 M. Baya, U. Belio, D. Campillo, I. Fernandez, S. Fuertes and A. Martin, Pt-M Complexes (M=Ag, Au) as Models for Intermediates in Transmetalation Processes, *Chem. – Eur. J.*, 2018, **24**, 13879–13889.
38 M. Baya, U. Belio, I. Fernandez, S. Fuertes and A. Martin, Unusual Metal-Metal Bonding in a Dinuclear Pt-Au Complex: Snapshot of a Transmetalation Process, *Angew. Chem., Int. Ed.*, 2016, **55**, 6978–6982.
39 D. Campillo, D. Escudero, M. Baya and A. Martin, Heteropolymetallic Architectures as Snapshots of Transmetallation Processes at Different Degrees of Transfer, *Chem. – Eur. J.*, 2022, **28**, e202104538.
40 R. J. Oeschger, R. Bissig and P. Chen, Model Compounds for Intermediates and Transition States in Sonogashira and Negishi Coupling: d(8)-d(10) Bonds in Large Heterobimetallic Complexes Are Weaker than Computational Chemistry Predicts, *J. Am. Chem. Soc.*, 2022, **144**, 10330–10343.
41 M. E. Moret, D. Serra, A. Bach and P. Chen, Transmetalation supported by a Pt(II)-Cu(I) bond, *Angew. Chem., Int. Ed.*, 2010, **49**, 2873–2877.
42 R. J. Oeschger, D. H. Ringger and P. Chen, Gas-Phase Investigations on the Transmetalation Step in Sonogashira Reactions, *Organometallics*, 2015, **34**, 3888–3892.
43 K. P. Bryliakov, E. P. Talsi, A. Z. Voskoboynikov, S. J. Lancaster and M. Bochmann, Formation and Structures of Hafnocene Complexes in MAO- and AlBui3/

CPh3[B(C6F5)4]-Activated Systems, *Organometallics*, 2008, **27**, 6333–6342.

44 M. Bochmann and S. J. Lancaster, Monomer–Dimer Equilibria in Homo- and Heterodinuclear Cationic Alkylzirconium Complexes and Their Role in Polymerization Catalysis, *Angew. Chem., Int. Ed. Engl.*, 1994, **33**, 1634–1637.

45 E. S. Cueny, H. C. Johnson and C. R. Landis, Selective Quench-Labeling of the Hafnium-Pyridyl Amido-Catalyzed Polymerization of 1-Octene in the Presence of Trialkyl-Aluminum Chain-Transfer Reagents, *ACS Catal.*, 2018, **8**, 11605–11614.

46 G. J. P. Britovsek, S. A. Cohen, V. C. Gibson and M. van Meurs, Iron Catalyzed Polyethylene Chain Growth on Zinc: A Study of the Factors Delineating Chain Transfer versus Catalyzed Chain Growth in Zinc and Related Metal Alkyl Systems, *J. Am. Chem. Soc.*, 2004, **126**, 10701–10712.

47 M. van Meurs, G. J. P. Britovsek, V. C. Gibson and S. A. Cohen, Polyethylene Chain Growth on Zinc Catalyzed by Olefin Polymerization Catalysts: A Comparative Investigation of Highly Active Catalyst Systems across the Transition Series, *J. Am. Chem. Soc.*, 2005, **127**, 9913–9923.

48 R. Marghalani and E. S. Cueny, Stability of metal–metal interactions in transmetallation intermediates based on electronics of bridging arene ligands determined through pyridine titrations, *Dalton Trans.*, 2024, **53**, 18839–18844.

49 K. Sangu, K. Fuchibe and T. Akiyama, A Novel Approach to 2-Arylated Quinolines: Electrocyclization of Alkynyl Imines via Vinylidene Complexes, *Org. Lett.*, 2004, **6**, 353–355.

50 Z. Zheng, G. Deng and Y. Liang, Synthesis of quinolines through copper-catalyzed intermolecular cyclization reaction from anilines and terminal acetylene esters, *RSC Adv.*, 2016, **6**, 103478–103481.

51 L. Yang, D. R. Powell and R. P. Houser, Structural variation in copper(i) complexes with pyridylmethylamide ligands: structural analysis with a new four-coordinate geometry index, τ4, *Dalton Trans.*, 2007, 955–964, DOI: 10.1039/B617136B.

52 H. E. Bryndza, L. K. Fong, R. A. Paciello, W. Tam and J. E. Bercaw, Relative metal-hydrogen, -oxygen, -nitrogen, and -carbon bond strengths for organoruthenium and organoplatinum compounds; equilibrium studies of Cp* (PMe3)2RuX and (DPPE)MePtX systems, *J. Am. Chem. Soc.*, 1987, **109**, 1444–1456.

53 E. Clot, M. Besora, F. Maseras, C. Mégret, O. Eisenstein, B. Oelckers and R. N. Perutz, Bond energy M–C/H–C correlations: dual theoretical and experimental approach to the sensitivity of M–C bond strength to substituents, *Chem. Commun.*, 2003, 490–491, DOI: 10.1039/B210036N.

54 S. Shekhar and J. F. Hartwig, Distinct Electronic Effects on Reductive Eliminations of Symmetrical and Unsymmetrical Bis-Aryl Platinum Complexes, *J. Am. Chem. Soc.*, 2004, **126**, 13016–13027.

55 R. S. Drago, *Physical Methods for Chemists*, Surfside Scientific Publishers, Gainesville, FL, 2nd edn, 1992, pp. 290–291.

56 B. E. Nadeau, D. D. Beattie, E. K. J. Lui, M. Tewkesbury, J. A. Love and L. L. Schafer, Electronic Directing Group Modification for Improved Ni(II)-Mediated C(sp3)–H Activation: A Hammett Investigation of 8-Aminoquinoline, *Organometallics*, 2023, **42**, 2326–2334.

57 P. Pyykkö, Strong Closed-Shell Interactions in Inorganic Chemistry, *Chem. Rev.*, 1997, **97**, 597–636.

58 H. Schmidbaur and A. Schier, Argentophilic Interactions, *Angew. Chem., Int. Ed.*, 2015, **54**, 746–784.

59 R. Dorel and A. M. Echavarren, Gold(I)-Catalyzed Activation of Alkynes for the Construction of Molecular Complexity, *Chem. Rev.*, 2015, **115**, 9028–9072.

60 C. Obradors and A. M. Echavarren, Intriguing mechanistic labyrinths in gold(i) catalysis, *Chem. Commun.*, 2014, **50**, 16–28.

61 (*a*) CCDC 2453724: Experimental Crystal Structure Determination, 2025, DOI: 10.5517/ccdc.csd.cc2nc9dr; (*b*) CCDC 2453725: Experimental Crystal Structure Determination, 2025, DOI: 10.5517/ccdc.csd.cc2nc9fs; (*c*) CCDC 2453726: Experimental Crystal Structure Determination, 2025, DOI: 10.5517/ccdc.csd.cc2nc9gt; (*d*) CCDC 2453727: Experimental Crystal Structure Determination, 2025, DOI: 10.5517/ccdc.csd.cc2nc9hv; (*e*) CCDC 2453728: Experimental Crystal Structure Determination, 2025, DOI: 10.5517/ccdc.csd.cc2nc9jw; (*f*) CCDC 2453729: Experimental Crystal Structure Determination, 2025, DOI: 10.5517/ccdc.csd.cc2nc9kx; (*g*) CCDC 2453730: Experimental Crystal Structure Determination, 2025, DOI: 10.5517/ccdc.csd.cc2nc9ly; (*h*) CCDC 2453731: Experimental Crystal Structure Determination, 2025, DOI: 10.5517/ccdc.csd.cc2nc9mz.